Electrostatic Interactions of Colloidal Particles at Vanishing Ionic Strength

Sunil K. Sainis, Jason W. Merrill, and Eric R. Dufresne*

Departments of Mechanical Engineering, Chemical Engineering, and Physics, Yale University, New Haven, Connecticut 06511

Received July 30, 2008. Revised Manuscript Received September 24, 2008

Electrostatic interactions of colloidal particles are typically screened by mobile ions in the solvent. We measure the forces between isolated pairs of colloidal polymer microspheres as the density of bulk ions vanishes. The ionic strength is controlled by varying the concentration of surfactant (NaAOT) in a nonpolar solvent (hexadecane). While interactions are well-described by the familiar screened-Coulomb form at high surfactant concentrations, they are experimentally indistinguishable from bare Coulomb interactions at low surfactant concentration. Interactions are strongest just above the critical micelle concentration, where particles can obtain high surface potentials without significant screening, $\kappa a \ll 1$. Exploiting the absence of significant charge renormalization, we are able to construct a simple thermodynamic model capturing the role of reverse micelles in charging the particle surface. These measurements provide novel access to electrostatic forces in the limit where the particle size is much less than the screening length, which is relevant not just to the nonpolar suspensions described here, but also to aqueous suspensions of nanoparticles.

1. Introduction

Electrostatic interactions determine the structure and stability of many colloidal dispersions. The classic theory of Derjaguin, Landau, Verwey, and Overbeek (DLVO)[1,2] rigorously describes the electrostatic interactions between charged particles when the electrostatic potential of the surface, ζ, is much less than k_BT/e. When the surface potential is large, Poisson−Boltzmann theory is used to describe the decay of the potential near the surface.[3] The DLVO form reemerges in the far field, where the center-to-center distance between the particles, r, is much greater than the screening length, κ^{-1}, albeit with a renormalized surface potential, ζ^*.[4−7]

The best probes of electrostatics in the nonlinear regime have come from the surface forces apparatus and atomic force microscope. These measurements focus on the limit of small separations, $r - 2a \ll a$, between large particles $\kappa a \gg 1$.[8,9] Here, were report measurements of electrostatic interactions between freely suspended colloidal particles in the opposite limit: vanishing ionic strength, $\kappa a \ll 1$.

While very low effective ionic strengths can readily be achieved with nanoparticles in common polar solvents, these particles are too small to observe and manipulate with visible light. Instead, we work with a suspension of microparticles in a nonpolar solvent. Specifically, we study the interactions of surfaces in nonpolar microemulsions of sodium aerosol-OT (AOT) in alkanes. The first measurements of electrostatic forces in such a solvent employed the surface forces apparatus to reveal interactions between macroscopic mica surfaces. They found a form of the interaction consistent with screening by counterions only.[10,11] Later, Hsu et al.[7] extracted the effective pair potential of micron-sized poly(methyl methacrylate) (PMMA) spheres confined to a monolayer by two PMMA-coated surfaces. The form of the pair potential was in good agreement with DLVO theory, but the ionic strength and effective surface potential were found to depend on the degree of confinement. Recently, we described the measurement of electrostatic forces between isolated pairs of micron-sized polymer (polystyrene and PMMA) particles using blinking optical tweezers.[12−14] We found good agreement with DLVO theory for a variety of particle compositions at ionic strengths with $\kappa a \approx 1$.

In this paper, we describe the interactions of micron-sized PMMA particles over a wide range of AOT concentrations. At the largest AOT concentrations, from 10^2 to 10^5 times the critical micelle concentration (CMC), we observe conventional DLVO interactions with $\kappa a \approx 1$, consistent with our earlier results.[7,13,14] From 10 CMC to 100 CMC, we find strong electrostatic interactions well fit by a bare Coulomb form. Conductivity measurements point to values of κa from 0.02 to 0.05, below the resolution of our interaction measurements. For AOT concentrations from zero to the CMC, we find very weak interactions just above our experimental resolution that are consistent with a Coulomb interaction with low surface potential, $|e\zeta^*| \approx k_BT$. Using direct numerical solution of the nonlinear Poisson−Boltzmann equation (NPBE) for isolated spheres with these values of ionic strength and apparent surface potential, we find that there is no significant charge renormalization. This insight facilitates the analysis of a simple physical picture for the strong increase of the surface potential just above the CMC.

* Corresponding author.

(1) Derjaguin, B. V.; Landau, L. *Acta Physicochim. URSS* **1941**, *14*, 633.
(2) Verwey, E. J. W.; Overbeek, J. T. G. *Theory of the Stability of Lyophobic Colloids: The Interactions of Sol Particles Having an Electric Double Layer*; Elsevier: New York, 1948.
(3) Hunter, R. J. *Foundations of Colloid Science*; Oxford University Press: New York, 2001.
(4) Alexander, S.; Chaikin, P. M.; Grant, P.; Morales, G. J.; Pincus, P.; Hone, D. *J. Chem. Phys.* **1984**, *80*, 5776.
(5) Netz, R. R.; Orland, H. *Eur. Phys. J. E* **2003**, *11*, 301.
(6) Trizac, E.; Bocquet, L.; Aubouy, M.; von Grunberg, H. H. *Langmuir* **2003**, *19*, 4027.
(7) Hsu, M. F.; Dufresne, E. R.; Weitz, D. A. *Langmuir* **2005**, *21*, 4881.
(8) Pashley, R. M.; Israelachvili, J. N. *J. Colloid Interface Sci.* **1984**, *97*, 446.
(9) Frechette, J.; Vanderlick, T. K. *Langmuir* **2001**, *17*, 7620.
(10) Briscoe, W. H.; Horn, R. G. *Langmuir* **2002**, *18*, 3945.
(11) Briscoe, W. H.; Attard, P. *J. Chem. Phys.* **2002**, *117*, 5452.
(12) Crocker, J. C.; Grier, D. G. *Phys. Rev. Lett.* **1994**, *73*, 352.
(13) Sainis, S. K.; Germain, V.; Dufresne, E. R. *Phys. Rev. Lett.* **2007**, *99*, 018303.
(14) Sainis, S. K.; Germain, V.; Mejean, C. O.; Dufresne, E. R. *Langmuir* **2008**, *24*, 1160.

10.1021/la8024606 CCC: $40.75
Published on Web 11/08/2008

2. Materials and Methods

2.1. Samples. We measure electrostatic interactions between isolated pairs of $a = 600$ nm radius PMMA microspheres coated with poly hydroxy-stearic-acid stabilizer synthesized by Andrew Schofield.[15] These particles are suspended at very low volume fractions of $\phi \approx 10^{-6}$ for interaction measurements.

Particles are suspended in solutions of sodium aerosol-OT (sodium di-2-ethylhexylsulfosuccinate or NaAOT) in hexadecane. Above the CMC, AOT forms nanometer-sized reverse-micelles containing about 20 surfactant molecules.[16] We chose hexadecane as a solvent because it absorbs relatively little water.[17] To further limit water absorption, we prepare and store our samples in a dry glovebox. We make no attempt to remove water that is in the reagents as received from the manufacturers. Experiments performed on samples prepared outside a glovebox show the same qualitative trends as reported here, but typically show different values of the surface potential. We measure the conductivity of AOT/hexadecane solutions with a commercial conductivity meter (Scientifica 600).

For interaction measurements, samples are loaded into glass sample cells fashioned out of three microscope coverslips mounted on a standard microscope slide. The glass surfaces are spin-coated with a 200−300 nm layer of PMMA−methacrylic acid (MAA). This coating helps to prevent the adsorption of PMMA spheres to the channel walls. The glass chamber is open to the atmosphere during interaction measurements.

2.2. Optical Microscopy and Micromanipulation. We image our samples in brightfield with an inverted optical microscope (Nikon TE2000). Images are recorded on a high speed digital video camera (Photron Fastcam 1024PCI) at a frame rate from 250 to 500 Hz. Images are magnified 150−375 times via the objective lens (100×, 1.4 N.A.) and relay optics.

We manipulate particles using holographic optical tweezers.[18−20] Particles are trapped with a 532 nm diode-pumped solid state laser (Coherent Verdi V-5). The laser wavefront is sculpted with a spatial light modulator (Holoeye LC-R-2500) to control the geometry and intensity of the traps near the focal plane. The trap laser light is blinked at 20 Hz using a chopper (Thorlabs MC1000A). A detailed discussion of the optical train and control system used in these experiments can be found in recent articles.[14,21]

2.3. Force Measurement. We extract interparticle forces from statistical properties of the trajectories of isolated pairs of beads. As described in greater detail elsewhere,[13] we repeatedly trap and release beads with blinking optical tweezers to thoroughly sample the stochastic dynamics of freely interacting particles. Provided that gradients in hydrodynamic coupling are not too strong, the short-time dynamics of particle trajectories are well-characterized by two kinematic parameters: the mean drift velocity, v, and the diffusion coefficient, D. These two quantities are related to the interparticle force, F, through a generalization of the Stokes−Einstein relation:

$$F = k_B T \frac{v}{D} \tag{1}$$

Thus, the spatial dependence of the kinematic parameters, $v(r)$ and $D(r)$ provide the interparticle force, $F(r)$.

An advantage of the present technique is that both v and D are measured directly from particle trajectories. In particular, the analysis does not depend on previous knowledge of the viscosity of the fluid or the radius of the particles.

2.4. Solution of Nonlinear Poisson−Boltzmann Equation. We numerically solved the NPBE for an isolated sphere using Mathematica. In this geometry, the NPBE reduces to an ordinary differential equation that can be directly integrated in the radial coordinate. We match the numerical solution of the NPBE to the Debye−Huckel solution in far-field, where the electrostatic energy of a simple ion is much less than $k_B T$.[30] Thus, given ζ^* and κ, we can extract the surface charge, Z, and the surface potential, ζ.

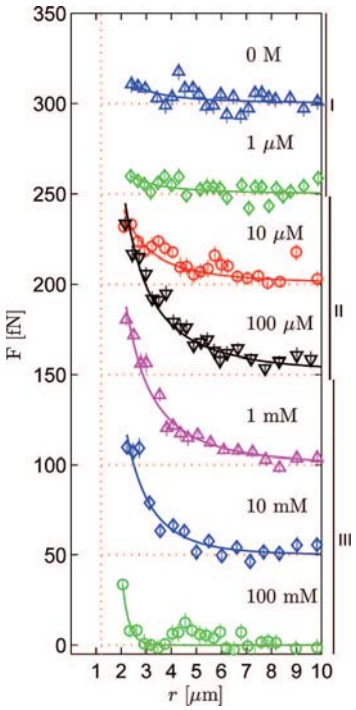

Figure 1. Electrostatic forces between charged colloidal particles in hexadecane for a wide range of AOT concentrations, as labeled. Forces for successive concentrations have been offset by 50 fN. Solid lines represent fits to screened-Coulomb interactions. Vertical and horizontal dashed red lines indicate particle−particle contact and zero force, respectively.

3. Results and Discussion

3.1. Interparticle Forces. The strength and range of interactions vary dramatically as the concentration of surfactant is varied, as shown in Figure 1. We observe three regimes of behavior. At low surfactant concentrations, from 0 M to 1 μM (Region I), we observe weak long-range repulsions just above our experimental resolution. For intermediate surfactant concentrations, from 1 μM to 100 μM (Region II), the repulsions increase monotonically with surfactant concentration. At high surfactant concentrations, from 1 mM to 100 mM (Region III), the range of the interactions decreases without significant changes to the force scale. The long-range nature of these forces suggests an electrostatic origin.

The force profiles are well fit by the electrostatic component of the DLVO interaction

$$\frac{F(r)}{F_o^D} = \frac{e^{-\kappa r}}{\kappa r}\left(\frac{1}{\kappa r} + 1\right) \tag{2}$$

where κ^{-1} is the Debye screening length, and F_o^D is the characteristic force, given by

$$F_o^D = \frac{k_B T}{\lambda_B}\left[\left(\frac{e\zeta^*}{k_B T}\right)\kappa a e^{\kappa a}\right]^2 \tag{3}$$

Note that the apparent surface potential observed in these interaction measurements, ζ^*, is expected to be smaller than the actual surface potential, ζ, because of nonlinear screening near the surface. The Bjerrum length, $\lambda_B = e^2/4\pi\varepsilon\varepsilon_o k_B T$, captures the

(15) Antl, L.; Goodwin, J. W.; Hill, R. D.; Ottewil, R. H.; Owens, S. M.; Papworth, S. *Colloids Surf.* **1986**, *17*, 67.
(16) Kotlarchyk, M.; Huang, J. S.; Chen, S. H. *J. Phys. Chem.* **1985**, *89*, 4382.
(17) Hou, M.-J.; Shah, D. O. *Langmuir* **1987**, *2*, 1086.
(18) Dufresne, E. R.; Grier, D. *Rev. Sci. Instrum.* **1998**, *69*, 1974.
(19) Dufresne, E. R.; Spalding, G. C.; Dearing, M. T.; Sheets, S. A.; Grier, D. G. *Rev. Sci. Instrum.* **2001**, *72*, 1810.
(20) Liesener, J.; Reicherter, M.; Haist, T.; Tiziani, H. J. *Opt. Commun.* **2000**, *185*, 77.
(21) Chapin, S. C.; Germain, V.; Dufresne, E. R. *Opt. Express* **2006**, *14*, 13095.

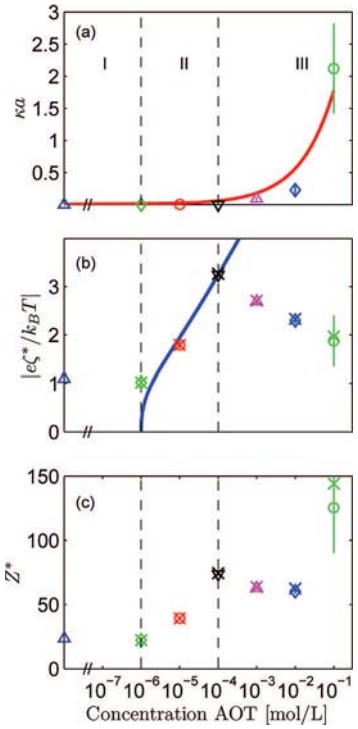

Figure 2. Ionic strength (a), surface potential (b), and charge (c) from fits to data in Figure 1. Effective zeta potential and charge are plotted as open symbols in panels b and c. Bare charge and zeta potential, calculated from data using the NPBE, are plotted with symbol × in panels b and c. Solid red line in panel a indicates estimate of ionic strength from conductivity measurements. Solid blue line in panel b indicates prediction of eq 10.

polarizability of the solvent; it is the separation where two elementary charges have an electrostatic interaction energy of k_BT. Verwey and Overbeek's original treatment includes additional terms in the force expression that become important for small separations and low ionic strength.[2] Differences in fit parameters resulting from fitting to their more complete form are well within experimental error, and so we present only the simpler form here. Specific values of the fitting parameters are plotted against surfactant concentration in Figure 2.

In Region III, these fits return κa and $|e\zeta^*/k_BT|$ on the order of unity. While the screening length and surface potential drop significantly as the surfactant concentration increases, the apparent surface charge,[4]

$$Z^* = \left|\frac{e\zeta^*}{k_BT}\right|\frac{a(1+\kappa a)}{\lambda_B} \tag{4}$$

is relatively constant.

In Regions I and II, we find that the inverse screening length, κ, is too small to reliably extract from a fit of the full DLVO form, so in these regions we fix $\kappa a = 0$ and fit to a bare Coulomb repulsion. The surface potential increases monotonically with surfactant concentration throughout Region II, as shown in Figure 2b, reaching a maximum of $|e\zeta^*/k_BT| = 3.25 \pm 0.05$ at 100 μM. With a combination of high surface potential and no measurable screening, there are significant interactions even at relatively large separations: particles feel a repulsion of 10 k_BT at a separation of 10 particle diameters.

As the surfactant concentration vanishes, the particles retain a small nonzero surface potential. Interaction forces are essentially identical at 0 M and 1 μM, where the particles show a measurable repulsion just above our experimental resolution. Both force curves are fit with $|e\zeta^*/k_BT| = 1.1 \pm 0.1$. This corresponds to a surface charge of about 23 ± 3 elementary charges. Thus, interfaces can charge even in the absence of charge control agents. Since no effort was made to purify the solvent, uncontrolled impurities may have facilitated charging. While the charge is not identically zero, the resulting forces are weak and could be insignificant in many contexts. Recent single particle electrokinetic measurements[22] extracted colloidal surface charges at high precision in an alkane. Their silica particles showed smaller charges, $Z \leq 11$, with intriguing dynamic fluctuations. Our force measurement, constructed from an average of particle fluctuations, essentially reports an average of the product of the charges of the two spheres.

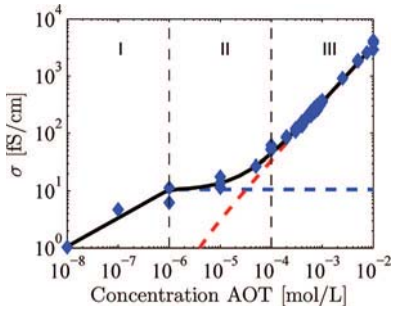

Figure 3. Conductivity of AOT/hexadecane solutions without particles. Symbols indicate measurements. Red dashed line indicates reverse micelle contribution to conductivity. Blue dashed line indicates surfactant monomer contribution to conductivity. Solid black line indicates sum of reverse micelle and monomer contributions.

One interesting facet of colloidal electrostatics at low κa is the absence of charge renormalization. It is well-known that the NPBE can be linearized in the limit where $|e\zeta| \ll k_BT$. However, the nonlinear term also becomes unimportant at vanishing ionic strength. We solved the NPBE for an isolated sphere to calculate the surface potential, ζ, and bare surface charge, Z, from observed values of the ionic strength and effective surface potential. The results of these calculations are plotted with symbol × in Figure 2b,c. For the sampled range of AOT concentrations, the differences between the bare and effective values of the surface potential and charge are smaller than the experimental uncertainty. Thus, we conclude that charge renormalization is insignificant at these low ionic strengths: $\zeta^* \approx \zeta$ and $Z^* \approx Z$. Theoretical papers have reached similar conclusions.[28,29,23]

3.2. Bulk Conductivity. The rapid increase in particle charge in Region II is triggered by the formation of reverse micelles. To monitor the concentration of reverse micelles, we measure bulk conductivity, σ, of AOT/hexadecane solutions using a commercial meter (Scientifica model 600). The growth of conductivity with surfactant concentration is shown in Figure 3. In Region I, the conductivity scales like $\sigma \sim [\mathrm{AOT}]^{1/2}$. The scaling transitions smoothly in Region II, and ultimately $\sigma \sim [\mathrm{AOT}]$ in Region III. In general, the conductivity, σ, is related to the ionic strength through

$$\sigma = \sum_i (z_i^2 e^2 n_i)/(6\pi\eta a_{hi}) \tag{5}$$

where η is the viscosity of the solvent, n_i, z_i, and a_{hi} are the number density, valence, and hydrodynamic radius of the ith

(22) Strubbe, F.; Beunis, F.; Neyts, K. *Phys. Rev. Lett.* **2008**, *100*, 218301.
(23) Belloni, L. *Colloids Surf., A* **1998**, *140*, 227.
(24) Eicke, H. F.; Borkovec, M.; Das-Gupta, B. *J. Phys. Chem.* **1989**, *93*, 314.
(25) Morrison, I. D. *Colloids Surf., A* **1993**, *71*, 1.
(26) Roberts, G. S.; Sanchez, R.; Kemp, R.; Wood, T. A.; Bartlett, P. *Langmuir* **2008**, *24*, 6530.
(27) Hayes, B. *Am. Sci.* **2005**, *93*, 104.
(28) Gronwall, T. H.; La Mer, V. K.; Sandved, K. *Phys. Z.* **1928**, *29*, 358.
(29) MacGillivray, A. D. *J. Theor. Biol.* **1969**, *23*, 205.
(30) Müller, H. *Kolloidchem. Beihefte* **1928**, *26*, 257.

ionic species. The conductivity in Region I is well-described by the dissociation of isolated surfactant molecules. For weak dissociation, the law of mass action requires that $[Na^+] = [AOT^-] \sim [NaAOT]^{1/2}$. In Region III, the conductivity is dominated by charge transport within reverse micelles (RM). Reverse micelles are aggregates of surfactant monomers that form above a critical concentration of monomer, called the CMC. Reverse micelles have highly polarizable cores, typically containing some absorbed water, which provide a relatively low electrostatic barrier to ionization, $g \approx \lambda_B/2a_c = 13k_BT$, where a_c is the radius of the polarizable core. Reverse micelles ionize by exchange of material during collisions with other reverse micelles.[7,24,25] The law of mass action requires that the ion density scales with the number density of reverse micelles: $[RM^+] = [RM^-] \sim [RM]$. The sum of monomer and micelle contributions to the conductivity quantitatively describes the data over all three regions. For [AOT] < CMC,

$$\sigma = \sigma_{CMC}\sqrt{[AOT]/CMC} \tag{6}$$

For [AOT] ≥ CMC,

$$\sigma = \sigma_{CMC} + \alpha([AOT] - CMC) \tag{7}$$

A fit of the data in Figure 3 gives the CMC and is plotted as a black line. The monomer and micelle contributions to the conductivity are plotted as dashed blue and red lines, respectively. The CMC lies at 1 μM, the border between Regions I and II.

We compare the ionic strengths estimated from our conductivity data to those determined from force measurements. While κ comes directly from fits to our force data, it can also be estimated from conductivity measurements. Debye−Huckel theory gives: $\kappa^2 = {}_i4\pi\lambda_B n_i$, where we assume monovalent ions. Using estimates for the mean hydrodynamic radii of AOT^- and Na^+ ions (0.5 nm), the mean radius of a reverse micelles (1.7 nm), and the number of AOT molecules per reverse micelle (20),[16] we estimate κ over the entire range of accessed AOT concentrations, as shown as a solid line in Figure 2a, including Regions I and II where interaction forces were indistinguishable from bare Coulomb interactions. We find fair agreement between these two approaches in Region III.

3.3. Charging Mechanism. The three distinct regions observed in force measurements are connected to the underlying dynamics of surfactant. In Region I, interparticle forces are weak and unaffected by the presence of isolated surfactant molecules. In Region II, the formation of reverse micelles in the bulk promotes surface charging without introducing significant screening. In Region III, interactions are screened and surface potentials drop as as the population of thermally ionized reverse micelles becomes significant.

In all cases, the surface potential is determined by thermodynamics. Here, we describe a simple thermodynamic model of charging at vanishing ionic strength by reverse micelle mediated dissociation. For a more detailed thermodynamic model, including competition of adsorption and dissociation, see the work of Roberts et al.[26] In our model, charging is driven by entropy: both the particle surface and solvent have more configurations in charged states. Simultaneously, charging is opposed by electrostatic forces. In thermodynamic equilibrium, the incremental increase in entropy is balanced by an incremental increase in electrostatic energy,

$$g_S + g_B + |e\zeta/k_BT| + \ln(Z/N_S) + \ln(Z/N_B) = 0 \tag{8}$$

Here, Z is the number of charges on the surface, g_S and g_B are the dimensionless self-energies of surface and bulk ions, $|e\zeta/k_BT|$ is the work needed to separate the incremental counterion from the surface, and N_S and N_B are the number of sites available for ions in the surface and bulk, respectively. We have assumed that the work to remove counterions is that to bring them to infinity, a good approximation for large double layers (small κa). In Region I, where surface charges and counterions are bare, their electrostatic self-energies are quite high $g_S \approx g_B \approx \lambda_B/2a_{ion} \approx 40k_BT$. Thus, entropy is only capable of weak charging of the interface. Evidently, the presence of surfactant monomer has no significant effect on the self-energies or ionic entropies.

We hypothesize that reverse micelles drive the charging of particles in Region II by accepting counterions into their polarizable cores, where their self-energy is relatively low. As reverse micelles are added to the system, there are more sites available to accept counterions, increasing the entropic incentive to charging and driving higher surface potentials. The physics is relatively simple in this context due to the paucity of bulk ions. Since there is no charge renormalization or screening, the particle surface potential is simply related to its charge by Coulomb's law: $|e\zeta/k_BT| = Z\lambda_B/a$. Thus, eq 8 can be solved without need for the Poisson−Boltzmann equation.

Assuming counterions must reside within reverse micelles, we find a simple algebraic expression for changes in the surface potential with reverse micelle concentration,

$$\left|\frac{e\zeta_2}{k_BT}\right| - \left|\frac{e\zeta_1}{k_BT}\right| + 2\ln\left[\frac{\zeta_2}{\zeta_1}\right] = \ln\left[\frac{n_2}{n_1}\right] \tag{9}$$

where ζ_1 and ζ_2 are the surface potentials at reverse micelle concentrations n_1 and n_2, respectively. This transcendental equation is readily solved for ζ at arbitrary reverse micelle concentrations, n, using the Lambert-W function, $W(x)$:[27]

$$\left|\frac{e\zeta}{k_BT}\right| = 2W\left\{\frac{1}{2}\left|\frac{e\zeta_o}{k_BT}\right|\exp\left[\frac{1}{2}\left|\frac{e\zeta_o}{k_BT}\right|\right]\left(\frac{n}{n_o}\right)^{\frac{1}{2}}\right\} \tag{10}$$

Here ζ_o is the surface potential at a reference reverse micelle concentration, n_o. Using the value of $|e\zeta/k_BT|$ at 100 μM AOT as a reference, we plot the predictions of eq 10 on top of our data in Figure 2b and find reasonable agreement with the sparsely sampled trend observed in Region II. This simple model does not describe the drop in surface potential observed in Region III. Here, the number of reverse micelles is large enough that their spontaneous self-ionization creates a significant background of free ions in the bulk. At these finite ionic strengths, a successful theoretical model must account for screening and charge renormalization and possibly the electrification of interfaces by ion adsorption.

4. Conclusion

We demonstrate strong electrostatic interactions between microparticles at vanishing ionic strength. We find that particles can interact with long-range forces indistinguishable from a bare Coulomb form. In the vanishing ionic strength regime, the physics of charging is quite simple due to a lack of charge renormalization. This, and other nonpolar colloidal systems, are well suited to the investigation of strongly correlated many-body systems, and provide convenient access to the $\kappa a < 1$ regime of colloidal electrostatics, also significant for aqueous nanocolloids.

Acknowledgment. This work was supported by the Cabot Corporation and the National Institute for Nano Engineering at Sandia National Laboratory. We thank Ian Morrison for helpful discussions. We thank Andrew Schofield for providing the PMMA particles and PHSA stabilizer.

LA8024606